Silica–Gold Core–Shell Nanosphere for Ultrafast Dynamic Nanothermometer

*Hongtao Sun, Xiang Sun, Mingpeng Yu, Ashish Kumar Mishra, Liping Huang, and Jie Lian**

Effective temperature measurements are of significance for a fundamental understanding of nanosystems and functional applications, requiring ultimate miniaturization of thermometers with reduced size but maintained sensitivity, simplicity, and accuracy of temperature reading. Grand challenges exist for scenarios of thermal shock or combustion where materials may be subjected to extreme thermal flux and drastic temperature variations, and dynamic thermal sensors with an ultrafast response are yet to be developed. Here, an innovative design of silica–gold core–shell (SiO_2@Au) nanospheres is demonstrated as a potential dynamic sensor with a sub-second response time and accurate temperature determination based on the strong temperature dependence of the thermally induced morphological self-reorganization and characteristic surface plasmon (SP) absorption of the metal shell. The irreversible thermally induced morphological and optical signatures behave as characteristic "fingerprints" for temperature recordings, allowing the retrieval of thermal history ex-situ. As compared with current nanothermometer technologies such as metal-filled nanotubes, the core–shell nanosphere-based dynamic thermosensor offers synergistic advantages of ultrafast time response, fast readout, permanent recording of thermal history, and ex-situ capabilities for effective temperature measurements.

1. Introduction

Nano-scale temperature control and accurate temperature measurements are very challenging for many energy and engineering-related applications in which materials of small experimental volumes may be used with high temperature gradients, and nanotechnologies maybe particularly useful in developing high-sensitivity temperature sensors. Various types of nanothermometers have been developed which are in general the miniaturization of the geometrical size of conventional thermometers with high spatial resolution and different sensing mechanisms.[1] These include liquid-in-tube nanothermometers based on temperature-dependent thermal expansion of liquids,[2–5] luminescent thermometers based on temperature-dependent emission intensity of semiconducting quantum dots (QDs),[6–8] nanoscale infrared (IR) thermometers from metal NPs based on blackbody radiation,[9] and Coulomb blockade nanothermometers from nano-sized superconductor-insulator-metal tunnel junctions based on the Coulomb blockade of tunneling.[10,11] Of particular importance, progresses have been achieved on the development of metal filled nanotube-based thermal sensors such as Ga/MgO, In/CNT, Ga/CNT, Au(Si)/Ga_2O_3, Pb/CNT, and Pb/ZnO nanosystems.[2–5,12,13] The temperature measurement based on thermal expansion of liquid or solid metals inside nanotubes relies on detailed microstructural characterization at the nanoscale, typically by in-situ transmission electron microscopy (TEM). They can be employed in a real time situation due to their restoration mechanisms after the thermal event thus called in-situ thermometers. Ex-situ measurements can be done by performing thermal treatment of the sensing materials and relocated into a TEM for microstructure characterization and temperature determination. The temperature calibration and determination by time-consuming TEM make the readout a slow process, and the metal filled nanotube nanothermometers typically display a slow time response (e.g., minutes or up to hours).[5]

Dynamic sensors based on nano/micro-sized particles are currently under active investigation with the sensing mechanisms based on different thermally-driven physical processes such as phase changes of crystalline materials (e.g., Eu-doped ZrO_2),[14] morphological/microstructural changes of nanostructures (e.g., Ag nanoparticles,[15] TiO_2 nanoparticles[16] and Au nano-thin films)[17] and thermally-stimulated recombination of electron–hole pairs in thermoluminenscence (TL) materials (e.g., commercial TL materials LiF:Mg,Ti, etc.).[18] The thermally driven physical process is irreversible, providing a pathway for permanently recording temperature history and allowing ex-situ characterization after thermal events. The thermally-driven physical processes can be rapidly measured

H. T. Sun, Dr. X. Sun, Dr. M. P. Yu, Prof. J. Lian
Department of Mechanical
Aerospace & Nuclear Engineering
Rensselaer Polytechnic Institute
Troy, New York, 12180, USA
E-mail: lianj@rpi.edu
Dr. A. K. Mishra, Prof. L. P. Huang
Department of Materials Science and Engineering
Rensselaer Polytechnic Institute
Troy, New York, 12180, USA

DOI: 10.1002/adfm.201303191

by spectroscopy techniques such as absorption, Raman, photoluminescence and thermoluminescence from the particles, making it possible for a fast readout. The dynamic sensors could potentially determine duration and temperature simultaneously as the thermally-induced physical processes are in general governed by the Boltzmann correlation ($e^{-E/kT}$) expressing the effect of temperature and the pre-exponential factor determining time dependence. However, these particle sensors display a response of the timescale of seconds or minutes and dynamic nanothermometers capable of ultrafast time response, e.g., in the sub-second time scale, are yet to be developed.

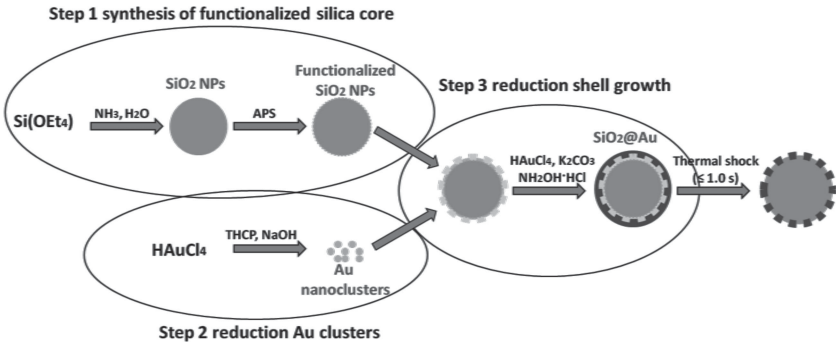

Scheme 1. A schematic representation of the synthesis procedure of SiO_2@Au nanospheres.

Here, we report an innovative dynamic nanothermometer based on a silica-gold core-shell (SiO_2@Au) nanosphere design with an ultrafast time response and accurate temperature reading. Metal nanoshells on dielectric or semiconducting cores typically display a strong optical resonance, highly dependent on the morphology of the shells and the core-to-shell ratios.[19,20] The plasmon resonance of the conduction electrons in the metal shell can lead to a large enhancement in local electric fields close to the metal surface which can be well explained by the classical electromagnetic theory (Mie theory).[21] As compared with the pure metal nanoparticles (NPs), metal shells have strong optical resonances that can be tuned over a much wider range by varying the shell coverage or the core-to-shell ratio. For instance, an absorption around 520 nm of gold NPs in the 5 nm size range in water shifts only 25 nm to larger wavelength with an increase in size to 80 nm.[20] While the resonance of gold nanoshells with a 120 nm diameter silica core can span a much larger range of 300 nm in wavelength as the core-to-shell ratio varies between 3 and 12.[19] The plasmon resonance of the conduction electrons for the metal nanoshell in a core-shell structure can cover almost anywhere across the ultraviolet, visible and infrared regions of the spectrum.[22] Due to their unique optical properties and extensive tunability, metal nanoshells can be employed in a range of very promising applications, e.g., optical imaging and labeling of biological systems,[23,24] optical sensing,[25–28] Raman spectroscopy enhancer,[29] optical filters,[30] and emission enhancer of ultraviolet LEDs.[31]

The operation principle of the novel SiO_2@Au dynamic nanothermometer is based on the temperature dependences of irreversible morphological instability and self-reorganization of nanoshells and characteristic surface plasmon (SP) absorption of the metal nanoshell. Particularly, upon thermal treatment, continuous nanoshell or partially-connected islands on non-wetted cores (such as silica) are metastable due to their high surface-to-volume ratios. Therefore, metal nanoshells decorated on dielectric cores can disintegrate and retract into arrays of equilibrium shaped NPs with a lower surface-to-volume ratio to reduce the surface area via the surface diffusion.[32–36] This process is driven by surface energy minimization and referred as solid state dewetting, which can generally occur well below melting temperature. The frequency and intensity of the localized surface plasmon (SP) bands are characteristics of materials and highly dependent on morphological characteristics such as particle size, size distribution, shape and coverage of the nanoshell as well as dielectric constants of the surrounding medium.[27,37] Therefore, the thermal history of the sensing materials experienced during a thermal event can be derived based on their characteristics of temperature-dependent SP absorption properties. In addition, the temperature dependent surface plasmon resonance (SPR) can be fast characterized by UV-vis-NIR spectrum,[17,38–40] enabling a fast readout for temperature determination.[41–44] As compared with the existing nanothermometer technologies, the core-shell structure enables ex-situ temperature measurements within a very fast time response (within sub-second time scale, 0.1–1.0 s) and also a fast readout.

2. Results and Discussion

The synthesis of the SiO_2@Au nanostructure is described in details in experimental section and the schematic representation of the synthesis process is illustrated in **Scheme 1**. To form a gold nanoshell, gold nanoclusters were first attached to the silica surfaces by gentle reduction of gold. The gold clusters attached to silica NPs were used as nucleation sites for further shell reduction, resulting in an increasing coverage of gold on the silica surface. During the shell growth, gold NPs began to coalesce on the silica surface, and finally gold nanoshells formed with controlled thicknesses and coverage (**Figure 1**), dependent on the amount of the precursor (gold nanoclusters decorated on silica cores) adding to the gold salt solution (Table S1, Supporting Information). This SiO_2@Au core-shell structure is characterized by the X-ray photoelectron spectroscopy (XPS) and X-ray diffraction (XRD) measurements, confirming the existence of SiO_2 and Au (Figure S1, Supporting Information).

The controllable coverage and thickness of gold nanoshells on silica cores result in tunable SP absorption bands in a wide range of wavelengths (the SP band wavelengths of samples 1–8 are also summarized in Table S1 in the Supporting Information). A continuous red shift in the SP band occurs as the coverage of gold nanoshell increases (**Figure 2**). As the gold NPs begin to coalesce and form partially connected islands on the silica surface (see sample 7 as shown in Figure 1d), their corresponding SP band becomes distorted into a broad shoulder (see Figure 2). Once reaching a complete shell coverage (sample 8 as shown in Figure 1e), the SP band shifts to a larger wavelength

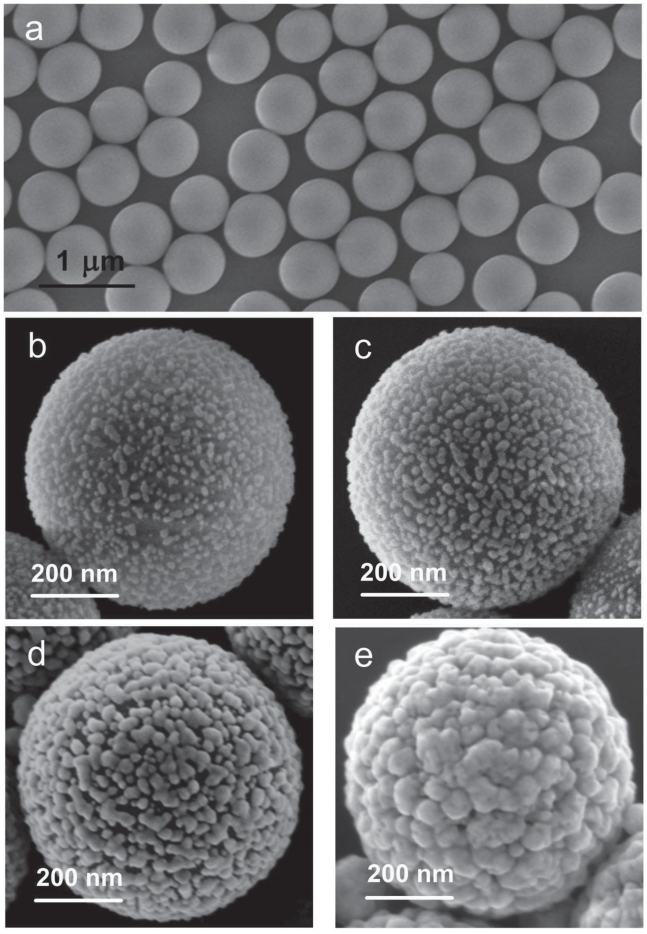

Figure 1. HR-SEM images showing morphology of SiO_2@Au nanostructures with different coverage: (a) silica spheres (617 ± 20 nm diameter); (b,c) silica cores with incomplete gold nanoshells (samples 1 and 3); (d) a quasi-complete gold nanoshell (sample 7); and (e) a complete gold nanoshell (sample 8).

(>1000 nm). Therefore, as the coverage of nanoshell increases, the SP band in UV-vis-NIR spectra increases in intensity and shifts toward longer wavelengths from 554 to 915 nm. These results demonstrate that different SiO_2@Au nanostructures can be fabricated with controlled morphologies and an extensive tunability of the SP absorption band, offering the possibility of designing nano-sized thermo-sensors with tunable sensitivity and time response.

It is essential that the synthesis of the SiO_2@Au nanostructure with controlled morphology and SP absorption can be reproducible in order to employ it as a potential thermometer for temperature sensing. Different batches of gold nanoshells were reproduced several times following the exactly same experimental procedure and conditions but with three different ratios of the precursor to the gold salt and the UV-vis-NIR spectra were acquired. As shown in Figure S2 (Supporting Information), the SP absorption band can be precisely controlled and highly reproducible by fine controlling the experimental conditions. The uncertainties for different batch samples are very small, e.g., 601.7 ± 2.1 nm wavelength for sample 3; 616.0 ± 2.8 nm for sample 4 and 752.5 ± 5.3 nm for sample 6 (Table S1, Supporting Information). These results demonstrate that the morphology of SiO_2@Au nanostructure and the characteristic SP absorption band can be well controlled.

The thermal response of the synthesized SiO_2@Au nanostructure as a potential ex-situ nanothermometer was tested from 300 to 800 °C upon thermal shock for different durations from 0.1 to 1.0 s using a CDS Analytical Pyroprobe 5000 heater, which can provide a well-controlled temperature profile and a rapid heating rate up to 20 000 °C s^{-1}. Before testing, materials with the consistent SP absorption band as characterized by UV-vis-NIR spectrometer were selected for thermal testing in order to minimize the experimental uncertainty in the thermal response of the sensing materials. The SiO_2@Au nanostructure (sample 3 in Table S1, Supporting Information) with a partial coverage of the nanoshell and initial SP band of around 602 nm was tested as an example to demonstrate the morphological self-reorganization upon thermal treatments and the variation of the characteristic SP absorption. Note that other samples with different coverage and initial SP band were also tested and show different temperature and time responses and thus different sensitivity as sensor materials for effective temperature measurements. Specifically, the sample with a thinner shell or less coverage is more energetically unstable and thus possesses a higher sensitivity to temperature variation due to a greater driving force (a lower energy barrier) for surface reorganization.

Figure 3 shows the morphological evolution of the SiO_2@Au nanostructure as examined by HR-SEM upon thermal shock for 0.1 s. Before thermal treatments, gold nanoshell displays an irregular shape upon the gold nanoparticle nucleation and coalescence on the silica spheres to form partially connected NPs (Figure 3a). Upon thermal treatments, gold NPs on the silica core experienced drastic shape changes varying with thermal shock temperatures, as caused by the thermal

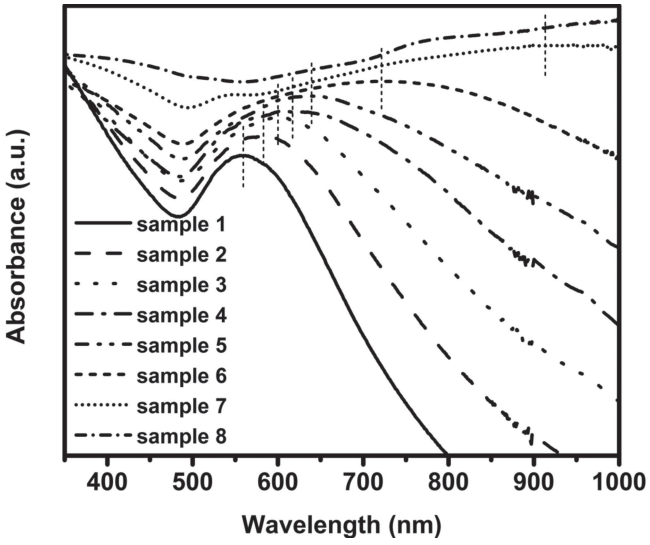

Figure 2. UV-vis-NIR spectra of the controllable gold nanoshell coverage on silica sphere of 617 ± 20 nm in diameter. The details of the synthetic parameters and SP band maxima for different samples are listed in Table S1 (Supporting Information).

dewetting-induced morphological instability driven by the surface diffusion to reduce the surface area and minimize the total energy of the system. Specifically, upon 300 °C thermal shock for 0.1 s (Figure 3b), gold nanoshell became less connected, and further increasing the thermal shock temperature to 400 °C (Figure 3c), the spacing of the interparticles was enlarged, resulting in a reduction of shell coverage. The irregular-shaped gold NPs became more regular upon 600 °C thermal shock (Figure 3d) and eventually disintegrated into isolated sphere shaped NPs with a lower surface-to-volume ratio upon 700 °C thermal shock. Similar morphological evolution was observed for the gold nanoshell upon 1.0 s thermal shock (Figure S3, Supporting Information). The establishment of the correlation between morphology (such as particle size, spacing and coverage area) and temperature provides the possibility for ex-situ temperature measurements based on the irreversible thermal-induced morphological self-organization. Note that in-situ temperature measurements using these SiO_2@Au sphere-based thermal sensors are feasible as well but time-consuming based on the temperature dependent morphology characteristics (e.g., in-situ heat and characterization inside a SEM or TEM).

The drastic morphological evolution of the gold nanoshell upon thermal dewetting significantly affects their optical properties as characterized by localized surface plasmon resonance (LSPR) spectroscopy, monitoring changes in SP absorption band in the visible spectral range. The characteristic SP absorption as controlled by the irreversible morphological variation can behave as fingerprint for ex-situ temperature recording with a fast readout. **Figures 4**a-c show the UV-vis-NIR spectra of gold nanoshells (sample 3) upon various thermal shock temperatures from 300 to 800 °C for 0.1, 0.5 and 1.0 s, respectively. All the UV-vis-NIR spectra illustrate a continuous blue shift attributed to the increase of the interparticle spacing and decrease of the shell coverage (Figure 3), and thus a weakening of the coupling effect with increasing thermal treatment temperatures from 300 to 800 °C. The blue shift of the SP band is consistent with our previous studies on ultrathin gold island films on quartz substrates upon various thermal treatment temperatures at longer durations (such as 180 s), in which the optical property variations of the island films or NPs are determined by the morphological characteristics.[17,39] Temperature-dependent absorption maxima of the SP bands are summarized in Figure 4d for different durations of 0.1, 0.5 and 1.0 s, and a continuous blue shift is clearly evidenced for all three cases. A significant SP band blue shift was observed for the core-shell structure within the temperature regime from 300~800 °C, even at the sub-second time frame (0.1 s). A similar temperature dependence on the SP band shift was observed for different durations. Temperature is a dominant factor impacting the morphological evolution and optical properties. A less time dependence can be identified and attributed to the extreme sensitivity of the nanoshell to thermal treatment in which the significant morphological reorganization is already completed within a very short time scale of 0.1 s. In addition to a sub-second time response, the core-shell structure also displays a high sensitivity for effective temperature measurement with a large SP band shift with temperature (e.g., 45 nm SP band shift in the temperature range from 300~800 °C, approximately 9 nm wavelength shift per 100 °C).

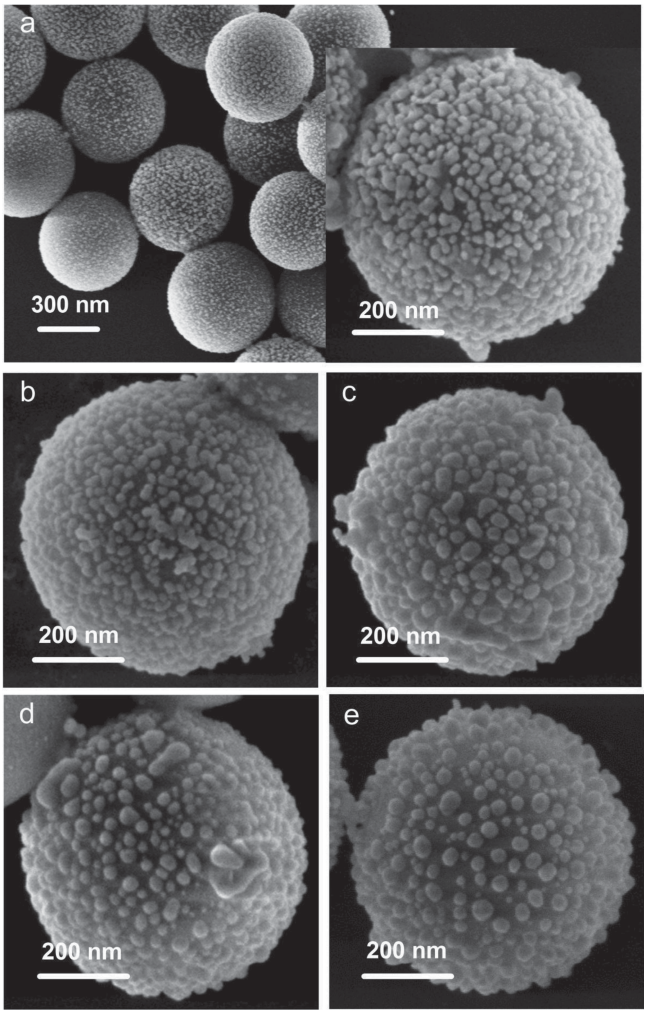

Figure 3. HR-SEM images showing morphological evolutions of the SiO_2@Au nanostructure (sample 3) upon thermal treatments at 0.1 s at different temperatures: (a) room temperature; (b) 300 °C; (c) 400 °C; (d) 600 °C; and (e) 700 °C. The silica-gold nanostructure with a partial gold shell coverage and initial SP band locating at ~602 nm was selected.

The time-dependent SP absorption band shift was plotted in **Figure 5**a for various thermal shock temperatures, and the time-dependent variations only occurred from 300 to 500 °C, especially for the time periods between 0.1 and 0.5 s. At a longer duration, the SP absorption band shift shows less time dependent, particularly at high temperature from 600~800 °C. Figure 5b shows the UV-vis-NIR spectra of the SiO_2@Au nanostructure upon thermal treatment at 500 °C with different durations from 0.1 to 2.0 s. Their corresponding time dependent absorption maxima of the SP bands are plotted and fitted as two linear functions in Figure 5c. The larger slope for the time periods from 0.0 to 0.3 s means a relatively higher sensitivity for time-dependent variations, and the variation of the SP band blue shift with durations between 0.3 and 2.0 s, suggesting less time dependent for morphology and the SP property variations.

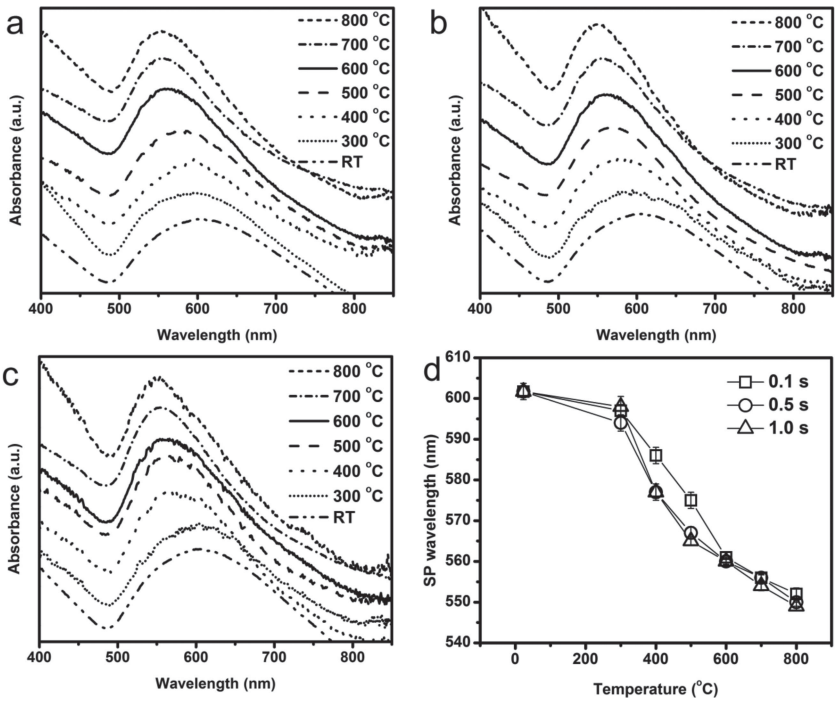

Figure 4. UV-vis-NIR spectra of gold nanoshells (sample 3) upon various thermal shock temperatures from 300 to 800 °C for 0.1 s (a), 0.5 s (b) and 1.0 s (c), and their corresponding temperature-dependent absorption maxima of SP bands (d).

The corresponding morphological evolution was demonstrated in the HR-SEM images (Figure S4, Supporting Information). The isolated gold NPs were formed on the silica core for all the time periods (0.1–2.0 s), and the coverage of gold nanoshell slightly decreased for the time periods more than 0.5 s leading to a slight blue shift of the SP bands in the UV-vis-NIR spectra.

The correlation of the SP absorption maxima as a function of temperature and duration provides the basis for designing the SiO_2@Au nanostructure-based thermal sensor for effective temperature measurement. Theoretically, both temperature and duration may be derived simultaneously by given two sensors (e.g., core-shell nanostructures with different gold shell coverage) based on their different thermal responses and thus different temperature and time dependences of the SP absorption band shift. A 3D fitting curve (shown in **Figure 6**a) can be built up using the third order polynomial approximation based on their time and temperature dependences, in which both temperature and duration are considered as variables affecting the SP band shift. Again, temperature is the dominant factor in controlling SP band shift, and a less duration dependence was observed particularly for the durations longer than 0.3 s, above which no significant SP bands shift was observed at greater temperatures. Due to the less time dependence, particularly for time periods more than 0.3 s, our SiO_2@Au core-shell nanostructure can be employed as an *ex-situ* nanothermometer for effective temperature measurement with a sub-second time scale for extreme thermal events. Specifically, temperature can be derived based on the two-dimensional (2-D) fitting curve of the temperature dependent SP band shift, assuming a time independence upon thermal shock for more than 0.3 s (Figure 6b). The temperature sensitivity (SP band shift per unit temperature, nm $°C^{-1}$) can be basically regarded as the slope of the tangent to the 2D fitting curve.

To validate the efficiency and accuracy in determining temperature as measured by the core-shell nanothermometer, control experiments were performed with the pre-set temperature and duration using the pyroprobe. The temperature the sensor materials experienced upon thermal shock from 400 to 800 °C can be calculated based on the temperature dependence of SP band shift (Figure 6b) and is cross-checked with the real temperature. As tabulated in **Table 1**, the calculated temperatures and corresponding uncertainties are listed respectively. These validations indicate that the 2D fitting curve enables accurate determination of temperatures within an uncertainty of 3%.

Table 1. Temperature measurements from the SP band variations.

Temperature [°C]	Calculated Temperature [°C]
400	398 ± 4
500	516 ± 17
600	597 ± 7
700	682 ± 26
800	800 ± 17

3. Conclusions

A potential dynamic nanothermometer was demonstrated based on SiO_2@Au nanostructure, capable of effective temperature recording with a sub-second response. A fast readout and temperature acquisition can be achieved by simply measuring the SP band shifts in the UV-vis-NIR spectra. The sensing mechanism is based on the temperature-dependent SP absorption band variation as a characteristic fingerprint for temperature recording tuned by the irreversible thermal dewetting-induced morphological changes. The sub-second time response (0.1–1.0 s) for the large range of temperature recording from 300 to 800 °C can be attributed to extreme sensitivity of the nano-scale shell structure and extensive tunability of its characteristic optical property. The silica-gold core-shell design offers immense potentials as ex-situ nanothermometers for effective temperature sensing with a sub-second response and fast readout for scenarios with an extreme thermal flux and drastic temperature change. The dimension of this novel dynamic thermal sensor, compatible with many nanosystems, may also offer the possibility of precise position for nano-scale temperature measurement.

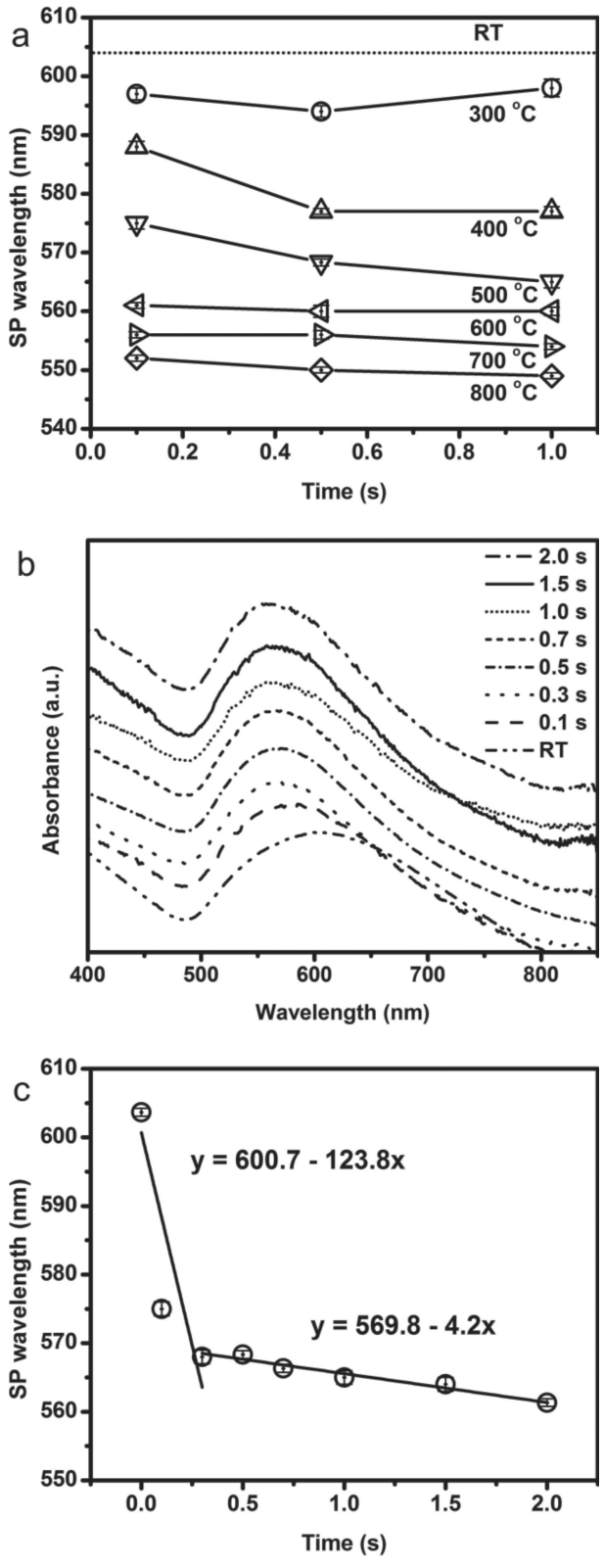

Figure 5. (a) Temperature and time-dependent absorption maxima of the SP bands for various thermal shock temperatures at different durations. (b) UV-vis-NIR spectra of time-dependent absorption for 500 °C thermal shock, and their corresponding time-dependent absorption maxima of the SP bands (c).

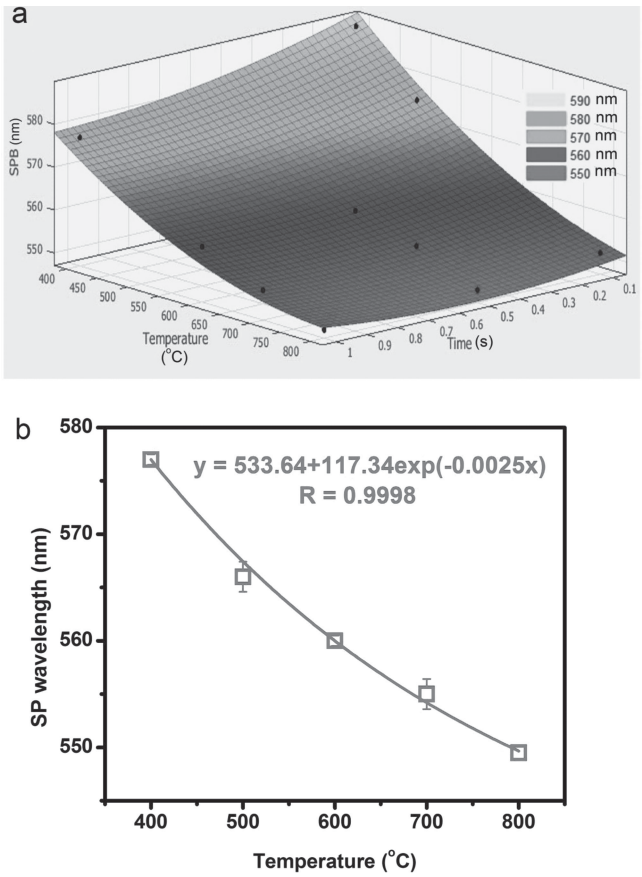

Figure 6. (a) A 3D fitting of absorption maxima of SP bands as a function of temperature and time. (b) A 2D fitting curve of absorption maxima of SP bands as a function of temperature. Assumption: time independence upon thermal shock for more than 0.3 s.

4. Experimental Section

Reagents: Tetraethoxysilane (TES, ≥98.0%), 3-aminopropyltrimethoxysilane (APS, ≥97.0%), tetrakis hydroxymethyl phosphonium chloride (THPC, 80.0%), hydroxylamine hydrochloride (99%), Potassium potassium carbonate (>99.0%) and gold (III) chloride hydrate (chloroauric acid) were purchased from Sigma-Aldrich. Ammonia solution (28.0–30.0 wt%) and sodium hydroxide were purchase from Fisher Scientific. All chemicals were used as received.

Synthesis: Gold functionalized silica particles were prepared using a modification of the method described by Oldenburg et al.[19] and Westcott et al.[45] Silica spheres were first obtained using the Stöber procedure.[46] A solution of ammonia (30 mL) and TES (4 mL) were added to dry ethanol (200 mL) under rapid stirring (> 150 rpm). The functionalization was carried out by mixing a certain amount of APS sufficient to provide an approximately 2.5 monolayer coatings on the silica particles. After stirred overnight, the solution was refluxed for 1 h to promote covalent bonding of the organosilane to the surface of the silica particles.[47,48] Excess reactants were removed from the APS-functionalized particles by centrifuging and re-dispersing in ethanol at least five times.

Aqueous solutions of small gold nanoclusters (1–2 nm in diameter) were prepared by reduction of chloroauric acid with THPC as described by Duff et al.[49] An appropriate amount of APS-functionalized silica particles was added dropwise into the freshly-prepared gold nanocluster solution and stirred for 12 h to form silica particle covered with the small gold clusters (precursor particles). Nonattached gold nanoclusters were removed by centrifuging and re-dispersing in water.

To initiate growth of the gold shell, silica particles attached gold nanoclusters were added to the aged mixture solution (gold hydroxide) of chloroauric acid and potassium carbonate.[20,50] The surface coverage or shell thickness depend on the ratio of the amount of the precursor particles to gold salt (see Table S1, Supporting Information). These suspensions were centrifuged to remove excess reagents for further characterization.

Thermal Treatment: Silica-gold core-shell NPs were undertaken sub-second (0.1~1.0 s) thermal shock from 300 to 800 °C on a platinum ribbon using a CDS Analytical Pyroprobe 5000 heater, with which the temperature can go up to 1400 °C and the rate may range from 0.01 °C/min to 20 000 °C/s. In this research, we always used the fastest heating rate to reach the target temperature. NPs were kept at certain temperature for certain amount of time before cooling down naturally in air when the power to the heater was turned off. Note that the as-synthesized samples were well dispersed in ethanol first before thermal treatments, and only one droplet of the solution was dispersed uniformly on the Pt foil for thermal shock testing to obtain a good thermal contact between particles and the heating element. The small amount of the SiO_2@Au nanospheres used (less than 5 mg) and a uniform dispersion on the Pt foil can assure a good thermal contact, and the effective heat transfer resulting from high thermal conductivity of the Au nanoshell can help to mitigate the non-uniformity in the temperature profile across nanospheres.

Material Characterization: X-ray diffraction (XRD) was performed using a PANanalytical x-ray diffraction system with the source wavelength of 1.542 Å at room temperature. X-ray photoelectron spectroscopy (XPS) was carried out using a PHI 5000 Versa Probe system. Absorption spectra were measured using a Varian Cary UV/VIS/NIR spectrophotometer with a scan rate of 600 nm min^{-1}, 1 nm interval and 0.1 s average measurement time per point. A baseline correction procedure was implemented prior to each measurement. High-resolution scanning electron microscopy (HR-SEM) images were obtained using a Carl Zeiss Supra SEM with a field emission electron source.

Supporting Information

Supporting Information is available from the Wiley Online Library or from the author.

Acknowledgements

This work is supported by DOD Defense Threat Reduction Agency (DTRA) under the grant of HDTRA1–10–1–0002. L. P. Huang also acknowledges the DTRA support (Grant Number HDTRA1–09–1–0046).

Received: September 13, 2013
Revised: October 24, 2013
Published online: December 20, 2013

[1] C. D. S. Brites, P. P. Lima, N. J. O. Silva, A. Millan, V. S. Amaral, F. Palacio, L. D. Carlos, *Nanoscale* **2012**, *4*, 4799.
[2] Y. H. Gao, Y. Bando, *Nature* **2002**, *415*, 599.
[3] N. W. Gong, M. Y. Lu, C. Y. Wang, Y. Chen, L. J. Chen, *Appl. Phys. Lett.* **2008**, *92*, 073101.
[4] Y. B. Li, Y. Bando, D. Golberg, Z. W. Liu, *Appl. Phys. Lett.* **2003**, *83*, 999.
[5] Y. H. Gao, Y. Bando, Z. W. Liu, D. Golberg, H. Nakanishi, *Appl. Phys. Lett.* **2003**, *83*, 2913.
[6] J. M. Yang, H. Yang, L. W. Lin, *ACS Nano* **2011**, *5*, 5067.
[7] C. H. Hsia, A. Wuttig, H. Yang, *ACS Nano* **2011**, *5*, 9511.
[8] S. Li, K. Zhang, J. M. Yang, L. W. Lin, H. Yang, *Nano Lett.* **2007**, *7*, 3102.
[9] M. G. Cerruti, M. Sauthier, D. Leonard, D. Liu, G. Duscher, D. L. Feldheim, S. Franzen, *Anal. Chem.* **2006**, *78*, 3282.
[10] D. R. Schmidt, C. S. Yung, A. N. Cleland, *Appl. Phys. Lett.* **2003**, *83*, 1002.
[11] A. T. Tilke, L. Pescini, H. Lorenz, R. H. Blick, *Appl. Phys. Lett.* **2003**, *82*, 3773.
[12] P. S. Dorozhkin, S. V. Tovstonog, D. Golberg, J. H. Zhan, Y. Ishikawa, M. Shiozawa, H. Nakanishi, K. Nakata, Y. Bando, *Small* **2005**, *1*, 1088.
[13] C. Y. Wang, N. W. Gong, L. J. Chen, *Adv. Mater.* **2008**, *20*, 4789.
[14] T. Myint, R. Gunawidjaja, H. Eilers, *J. Phys. Chem. C* **2012**, *116*, 21629.
[15] Y. C. Lan, H. Wang, X. Y. Chen, D. Z. Wang, G. Chen, Z. F. Ren, *Adv. Mater.* **2009**, *21*, 4839.
[16] J. W. Wang, L. P. Huang, *Appl. Phys. Lett.* **2011**, *98*, 113102.
[17] H. T. Sun, M. P. Yu, X. Sun, G. K. Wang, J. Lian, *J. Phys. Chem. C* **2013**, *117*, 3366.
[18] E. G. Yukihara, E. D. Milliken, L. C. Oliveira, V. R. Orante-Barron, L. G. Jacobsohn, M. W. Blair, *J. Lumin.* **2013**, *133*, 203.
[19] S. J. Oldenburg, R. D. Averitt, S. L. Westcott, N. J. Halas, *J. Chem. Phys. Lett.* **1998**, *288*, 243.
[20] C. Graf, A. van Blaaderen, *Langmuir* **2002**, *18*, 524.
[21] G. Mie, *Ann. Phys.* **1908**, *25*, 377.
[22] A. E. Neeves, M. H. Birnboim, *J. Opt. Soc. Am. B* **1989**, *6*, 787.
[23] K. Sokolov, M. Follen, J. Aaron, I. Pavlova, A. Malpica, R. Lotan, R. Richards-Kortum, *Cancer Res.* **2003**, *63*, 1999.
[24] I. H. El-Sayed, X. H. Huang, M. A. El-Sayed, *Nano Lett.* **2005**, *5*, 829.
[25] A. J. Haes, L. Chang, W. L. Klein, R. P. Van Duyne, *J. Am. Chem. Soc.* **2005**, *127*, 2264.
[26] K. S. Lee, M. A. El-Sayed, *J. Phys. Chem. B* **2006**, *110*, 19220.
[27] S. Underwood, P. Mulvaney, *Langmuir* **1994**, *10*, 3427.
[28] P. K. Jain, M. A. Ei-Sayed, *J. Phys. Chem. C* **2007**, *111*, 17451.
[29] S. M. Nie, S. R. Emery, *Science* **1997**, *275*, 1102.
[30] Y. Dirix, C. Bastiaansen, W. Caseri, P. Smith, *Adv. Mater.* **1999**, *11*, 223.
[31] D. L. Shao, H. T. Sun, M. P. Yu, J. Lian, S. Sawyer, *Nano Lett.* **2012**, *12*, 5840.
[32] W. W. Mullins, *J. Appl. Phys.* **1957**, *28*, 333.
[33] D. J. Srolovitz, S. A. Safran, *J. Appl. Phys.* **1986**, *60*, 247.
[34] E. Jiran, C. V. Thompson, *J. Electron. Mater.* **1990**, *19*, 1153.
[35] D. J. Srolovitz, S. A. Safran, *J. Appl. Phys.* **1986**, *60*, 255.
[36] E. Jiran, C. V. Thompson, *Thin Solid Films* **1992**, *208*, 23.
[37] P. Mulvaney, *Langmuir* **1996**, *12*, 788.
[38] T. Karakouz, D. Holder, M. Goomanovsky, A. Vaskevich, I. Rubinstein, *Chem. Mater.* **2009**, *21*, 5875.
[39] H. T. Sun, M. P. Yu, G. K. Wang, X. Sun, J. Lian, *J. Phys. Chem. C* **2012**, *116*, 9000.
[40] A. B. Tesler, L. Chuntonov, T. Karakouz, T. A. Bendikov, G. Haran, A. Vaskevich, I. Rubinstein, *J. Phys. Chem. C* **2011**, *115*, 24642.
[41] X. M. Zhang, J. H. Zhang, H. A. Wang, Y. D. Hao, X. Zhang, T. Q. Wang, Y. N. Wang, R. Zhao, H. Zhang, B. Yang, *Nanotechnology* **2010**, *21*, 465702.
[42] I. Doron-Mor, Z. Barkay, N. Filip-Granit, A. Vaskevich, I. Rubinstein, *Chem. Mater.* **2004**, *16*, 3476.
[43] A. Goyal, J. Narayan, Q. H. Lin, *J. Mater. Res.* **2011**, *26*, 109.
[44] T. Dehoux, T. A. Kelf, M. Tomoda, O. Matsuda, O. B. Wright, K. Ueno, Y. Nishijima, S. Juodkazis, H. Misawa, V. Tournat, V. E. Gusev, *Opt. Lett.* **2010**, *35*, 940.
[45] S. L. Westcott, S. J. Oldenburg, T. R. Lee, N. J. Halas, *Langmuir* **1998**, *14*, 5396.
[46] W. Stober, A. Fink, E. Bohn, *J. Colloid Interface Sci.* **1968**, *26*, 62.
[47] A. Vanblaaderen, A. Vrij, *J. Colloid Interface Sci.* **1993**, *156*, 1.
[48] T. G. Waddell, D. E. Leyden, M. T. Debello, *J. Am. Chem. Soc.* **1981**, *103*, 5303.
[49] D. G. Duff, A. Baiker, P. P. Edwards, *Langmuir* **1993**, *9*, 2301.
[50] D. G. Duff, A. Baiker, I. Gameson, P. P. Edwards, *Langmuir* **1993**, *9*, 2310.